Proceedings of 13th European Conference on Turbomachinery Fluid dynamics
Paper ID: ETC2019-218 & Thermodynamics ETC13, April 8-12, 2019; Lausanne, Switzerland

ROBUST INTEGRATION OF REAL GAS MODELS INTO A PRESSURE-BASED COUPLED SOLVER

L. Hanimann, L. Mangani, E. Casartelli

University of Applied Sciences Lucerne
Technik & Architektur
Technikumstrasse 21
6048, Horw
Switzerland
lucian.hanimann@hslu.ch

D. Vogt

University of Stuttgart
Institute of Thermal Turbomachinery and Machinery Laboratory
Paffenwaldring 6
70569 Stuttgart
Germany

ABSTRACT

Today's most common standard for compressible computational fluid dynamics is based on the ideal gas state equation. However, real gas modeling is fundamental for a wide range of applications. When expanding into the thermodynamic region of non-ideal gas, performance predictions based on ideal gas assumption are no longer valid. Therefore, more accurate models are desired for an improved classification of fluid properties. While there is a wast amount of literature about possible improvements when using real gas state equations in a numerical framework, little is known considering the actual implementation. This article will therefore focus on the robust integration of real gas flow physics in an in-house, coupled, pressure-based solver. We will point out the main difference to a numerical framework purely based on perfect gas. Final validation is given using a two stage radial compressor setup to demonstrate the generality of the chosen approach.

KEYWORDS: Real Gas, Numerical, Compressor

NOMENCLATURE

c_v, c_p specific internal energy
D reference diameter
e internal energy
F body forces
f frequency
h enthalpy
$\dot{m}$ Mass flow
p pressure
R_s specific gas constant
s entropy
S_f surface vector
t time
T temperature
u velocity
U velocity flux
v specific volume
V cell volume
z Compressibility

Greek
α attraction coefficient
$\dot{V}$ volume flow
η efficiency
κ conductivity or acentric factor
λ work coefficient
μ dynamic viscosity
ρ density
τ stress tensor

Superscripts
$*$ old time step values

Subscripts
c critical point values
r reference point values
f face values
0 total condition values
p polytropic value
i, j coordinate index
v_∞ ideal gas state

OPEN ACCESS
Downloaded from www.euroturbo.eu

Copyright © by the Authors

INTRODUCTION

The use of CFD for the prediction of flow physics has become a standard for industrial and scientific applications. Especially for turbomachinery design, the complexity of the investigated applications has increased drastically over the past decades. This is partly due to the size of the computational domain for multistage configurations, rotor-stator interactions due to various rotating and moving parts but also due to the wide range of operating conditions. In order to simplify the complexity of the numerical calculations it is therefore often assumed that the working fluid follows the approximations of an idealized gas. While for many applications this assumption can be justified there is an increasing demand for more accurate representation of the thermophysical properties.

The applications in question share the fact that the operating conditions are too far away from the ideal gas state. Associated thermophysical states do no longer allow the assumption of negligible intermolecular forces, hence suitable models for their accurate representation need to be applied. Low pressure stages in steam turbines (Starzmann et al. (2014)) or ORC turbines (Colonna et al. (2006)) are examples of applications that operate either fully or partly in the non-ideal state.

Many authors have investigated the impact of various real gas models, mainly focusing on possible achievements in the accuracy of the results and the impact on computational time due to the increased complexity of the thermophysical models, see e.g. Pohl et al. (2013), Odabaee et al. (2016), Boncinelli et al. (2003), Colonna et al. (2006). Reasons for the increase in computational time are manifold. It is not only due to the directly visible increased complexity of the state equations, but also due to the accompanied need for iterative solution procedures in the update of properties, as will be shown later. This drawback is often addressed by the use of lookup tables as shown by Boncinelli et al. (2003). Generation of these databases is however not straightforward, since the user needs to know in advance the range of thermophysical states which can be cumbersome for certain applications. Additionally the user needs to decide on the resolution of the generated table data. Low resolution may lead to a faster numerical procedure, but can diminish the quality of the results. Ameli et al. (2018) demonstrated the high sensitivity of the results to lookup table resolution. The presented framework will therefore use algebraic relations, however replacement with pre-tabulated data is straightforward and does not reduce the generality of the chosen derivations.

While there is a wast amount of literature about possible improvements in accuracy of the numerical solutions when choosing real gas state equations, little is known concerning the actual implementation into a numerical framework and possible sources for the reason of the increased computational time. Some numerical detail has been presented in Travis et al. (2013) or Lucas et al. (2014). The authors will therefore quickly point out the applied models for the integration of real gas models into an in-house numerical framework, see Mangani et al. (2014*a*,*b*, 2016). The used framework is based on a fully-coupled pressure based solution strategy for incompressible and compressible flows at any speed. We will point out the main differences compared to a framework purely derived for perfect gas and explain the reasons for the increase in computational time. Focus is on the differences in the derivation of conservation equations and boundary conditions as well as the update of thermophysical properties compared to the idealized gas state equations. Although the derivation is general for any real gas, we will give more detailed derivation for the cubic state equations, e.g. Peng & Robinson (1976).

The implemented solution procedure is then validated using an industrial type two stage compressor at one operational speed for the full range from chocking flow to the stability limit.

NUMERICAL ENVIRONMENT

This section provides a basic understanding to what is referred here as a pressure based coupled solution strategy for linearized finite volume equations in correction form. To the present day, literature on the numerical solution procedures of RANS equations is primarily based on methods generally known as segregated solution strategies, e.tg the SIMPLE family of algorithms. These algorithms solve the conservation equations in a sequential fashion, i.e. only solving for a single scalar quantity while keeping all other properties constant. This has historical reasons and is mainly due to restrictions in computer memory and the ease of implementation. Major drawback of these methods are a slow convergence behavior due to the decoupling of the pressure and velocity field which are naturally strongly coupled. Recent developments in computer architecture however have opened the opportunity to solve these fields simultaneously. This is usually known as the coupled solution procedure. An in-house framework has been developed and successfully tested by Mangani et al. (2014*a*,*b*, 2016). Since a complete derivation of the coupled solution strategy would go beyond the scope of this article, we will focus on the difference when integrating real gas state equations.

REAL GAS THEORY

Real gases are compositions of materials at thermophysical states under which its molecules are dense enough to allow intermolecular forces. This is in contrast to the theory of perfect gases where these forces are small enough to be neglected. Use of the perfect gas model has many advantages, considering the numerical discretisation of the RANS equations. Not only do the equations them self simplify but also many underlying derivations as the update of boundary values or the computation of primitive variables like temperature and density.

When using perfect gas state equations it is assumed that any change in the properties of the material behaves as if for infinitesimally high specific volume (far right of the T-v diagram in Fig. 1, line B). This justifies the assumption of negligible intermolecular forces.

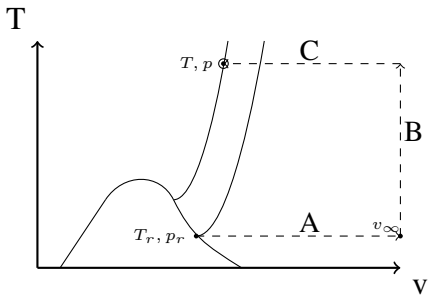

Figure 1: **Integration path**

It is clear that this is an idealized assumption and does not apply for a wide range of applications. When temperature and pressure changes the underlying thermophysical relationsships need to account for the real change. An example is the change in internal energy. Using the first and second law of thermodynamics, the total change in internal energy due to a change in

temperature and pressure is given as shown in Eq. 1

$$de = c_v dT + \left[T \left(\frac{\partial p}{\partial T} \right)_v - p \right] dv \tag{1}$$

To compute the value of $e(T, p)$ we use an integration along the paths A - B - C in Fig. 1. Given the reference state $e(T_r, p_r)$ the current value of internal energy is therefore computed as given in Eq. 2.

$$\begin{aligned} e(T,p) = & \underbrace{\int_{v_r}^{v_\infty} \left[T \left(\frac{\partial p}{\partial T} \right)_v - p \right]_{T_r} dv}_{A} + \underbrace{\int_{T_r}^{T} \left[c_v \right]_{v_\infty} dT}_{B} \\ & + \underbrace{\int_{v_\infty}^{v} \left[T \left(\frac{\partial p}{\partial T} \right)_v - p \right]_{T} dv}_{C} + e(T_r, p_r) \end{aligned} \tag{2}$$

No assumptions in the derivation are applied allowing for a generalized procedure for any kind of chosen state equations. For ideal gas, term A and C vanish as can be easily seen. Term B can be modelled e.g. using the assumption of a calorically perfect gas (i.e. c_v = ∉) or any other model e.g. NASA's polynomial approach (McBride et al. (2002)). Detailed derivation of the algebraic expression for the update of internal energy is given in the next section using the cubic state equation as given by Peng & Robinson (1976).

Cubic state equations

Cubic state equations are a family of state equations describing the change in pressure as a cubic function of the specific volume. Based on its ancestor, the Van der Waals state equation, many variations have emerged over the past decades to overcome some of it's drawbacks. Modifications have been applied to improve the phase transition by Soave (1972) or the prediction of liquid phase density and accuracy in the critical region by Peng & Robinson (1976). Both formulations have become an industrial standard and have therefore been used for the presented validation test case setup. The differences in the solutions between the two state equations are however small. Hence we will focus on the results obtained with the Peng-Robinson state equation. The cubic state equation is given as Eq. 3, with a and b being model coefficients.

$$p = \frac{R_s T}{v - b} - \frac{a\alpha^2}{v^2 + 2bv - b^2} \qquad \alpha = \alpha(T) = 1 + \kappa \left(1 - \sqrt{\frac{T}{T_c}} \right) \tag{3}$$

Using the above described integration by paths, the value of internal energy can be computed as given in Eq. 4

$$\begin{aligned} e(T,v) = & \frac{a\alpha(T_r)(1+\kappa)}{\sqrt{2}b} tanh^{-1} \left(\frac{\sqrt{2}b}{b + v_r} \right) + \frac{a\alpha(T)(1+\kappa)}{\sqrt{2}b} tanh^{-1} \left(\frac{\sqrt{2}b}{b + v} \right) \\ & + \int_{T_r}^{T} \left[c_p \right]_{v_\infty} dT - R_s (T - T_r) + e(T_r, v_r) \end{aligned} \tag{4}$$

Similar procedure do apply for any cubic state equations and other properties as the update of entropy which is e.g. needed for total condition boundaries as shown later. Further information and algebraic expressions for the update of properties based on real gas thermophysic behaviour can be found in Nederstigt (2017) in chapter 11.

REAL GAS NAVIER STOKES EQUATIONS

In the following sections we are going to point out the major challenges in the derivation of conservation equations when moving to real gas state equations.

Momentum Equation

The momentum equation is given in Eq. 5. Considering the implementation of real gas, no changes are necessary.

$$V\left(\frac{\partial \rho u_i}{\partial t} - F_{bi}\right) + \sum_f \left(\left(\rho_f u_{fj} u_{fi}\right) + p_f - \left(\tau_{fij}\right)\right) S_{fi} = 0 \tag{5}$$

Continuity equation

The continuity equation is used to obtain an equation for the pressure which serves as a constrained to fulfill the conservation of mass. Eq. 6 shows the continuity equation in its semi discrete form with $U_f = u_{fi} S_{fi}$ being the velocity flux across the face.

$$V\frac{d\rho}{dt} + \Sigma_f \rho_f U_f = 0 \tag{6}$$

To expand the first part of the equation, the temporal derivative, it is considered the general assumption that the density is a function of pressure and enthalpy, see Lucas et al. (2014). It is therefore linearized as given in Eq. 7.

$$\frac{d\rho}{dt} = \left(\frac{\partial \rho}{\partial h}\right)_p \frac{dh}{dt} + \left(\frac{\partial \rho}{\partial p}\right)_h \frac{dp}{dt} \tag{7}$$

The second term of the continuity equation, the convective contribution, is discretized using Newton linearization, see Eq. 8.

$$\rho_f U_f = \rho_f^* U_f + \rho_f U_f^* - \rho_f^* U_f^* \tag{8}$$

To avoid checkerboarding pressure fields on collocated arrangements and to introduce the necessary implicit dependency on pressure and the coupling of the continuity to the momentum equation, the velocity flux of the new time step (U_f) is computed using Rhie & Chow (1983) interpolation technique.The value of the density on the face (ρ_f) is approximated by a first order linearization leading to yet another implicit dependency on pressure, see Eq. 9

$$\rho_f = \rho_f^* + \left(\frac{\partial \rho}{\partial p}\right)_{hf} (h_f - h_f^*) + \left(\frac{\partial \rho}{\partial h}\right)_{pf} (p_f - p_f^*) \tag{9}$$

Compared to a derivation using ideal gas assumptions, we account for the dependency of density on pressure and enthalpy. Main difference is however the derivation of the partial derivatives due to the change in state equation.

Energy equation

The energy equation is given in terms of total enthalpy in Eq. 10.

$$V\left(\frac{\partial \rho h_0}{\partial t} - \frac{\partial p}{\partial t}\right) + \sum_f \left(\rho_f u_{fi} h_{0f} - \kappa_f \frac{\partial T}{\partial x_i} - u_{fj} \tau_{fij}\right) S_{fi} = 0 \tag{10}$$

In the presented framework, all equations are solved in a correction form. Hence the linearized system is not solved for the value of the current time step, but for the correction of the previous solution. The heat conduction in the form given above would however add a completely explicit contribution to the source of the system of equations, diminishing the stability of the iterative solution procedure. Different to ideal gas state equations, the enthalpy is not only a function of temperature but also depends on the pressure level. The temperature of the actual time step is therefore approximated using a first order linearization, leading to Eq. 11.

$$\sum_f -\kappa_f \left(\frac{\partial T}{\partial x_i}\right)_f S_{if} = \sum_f (-\kappa_f \left(\frac{\partial T^*}{\partial x_i}\right)_f - \underbrace{\frac{\kappa_f}{c_{pf}} \left(\frac{\partial h'_f}{\partial x_i}\right)_f}_{a} + \underbrace{\kappa_f \frac{h'_f}{c_{pf}^2} \left(\frac{\partial c_p}{\partial x_i}\right)_f}_{b}) \cdot S_{if} \quad (11)$$

The implicit dependency on the correction of enthalpy leads to an increased diagonally dominance of the coefficient matrix, stabilizing the iterative solution procedure.

ITERATIVE PROCEDURE FOR PROPERTIES UPDATE

With the velocity, pressure and the total enthalpy being evaluated during the solution of the Navier-Stokes equations, many other thermophysical quantities need to be evaluated based on these solutions. While some of these quantities are a necessity for the overall iterative solution procedures (e.g. density and temperature), others are purely for post processing reasons. For perfect gas, the evaluation of these variables pose no challenge, since all of them can be directly evaluated through well known algebraic relations. Using real gas models, this is no longer possible. Either because the given equation allows for multiple solution, e.g. when computing the density based on temperature and pressure given the cubic state equation, or because there is simply no algebraic relation as in the case of static to stagnation conversion as needed specified total conditions boundary condition. Given the static values of p and T the entropy can be computed using a similar integration along paths as given in Eq. 2. What is searched for are a combination of T_0, p_0 such that $s(T, p) = s(T_0, p_0)$. The second constrained is that the enthalpy computed using T_0, p_0 is equal to the solution given from the energy equation. This problem is solved using Newton-Raphson root finding algorithm with the roots given in Eq. 13.

$$s(T, p) - s(T_0, p_0) = 0 \quad (12)$$

$$h(T_0, p_0) - h_0 = 0 \quad (13)$$

VALIDATION

The test case for the validation setup is a two-stage radial compressor. Governmental requirements on the GWP (Global Warming Potential) of the refrigerant required a switch of the working fluid. This lead to a redesign of the components accompanied with measurements herein used for the validation of the implemented numerical model. Apart of the general redesign, the main objective of the measurement campaign was to gain information on the surge line under various operating conditions to allow for a controlled operation of the compressor. A vaneless radial diffuser follows each impeller while the return channel contains a single row of stationary blades to reduce the swirl before the second impeller. Figure 2 shows the individual parts.

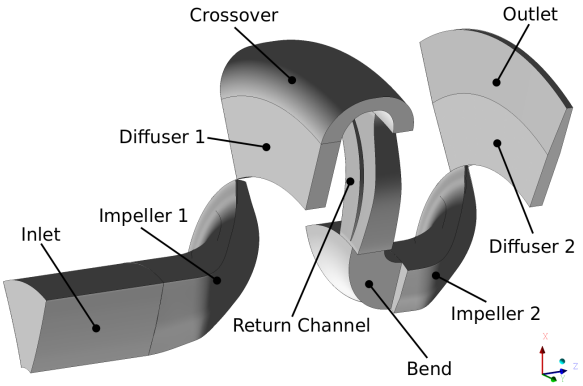

Figure 2: **Parts Overview**

Measurement Setup

The two stage compressor was installed in the laboratory of the institute for thermal energy system and process engineering at HSLU in Lucerne. Restriction in the laboratory environment however led to operating conditions which are not in line with the design. This concerns mainly the inlet temperature and pressure levels, which could not be tuned to design conditions.
In order to account for this inconsistency, dynamic scaling was applied to match the operating conditions of the design. The rotational speed of the compressor was corrected using in Eq. 14, with f being the design frequency and f' the corrected frequency of the laboratory setup. The mass flow is then corrected based on the non-dimensional mass flow as given in Eq. 14 for comparison with the design conditions.

$$f' = \frac{f}{\sqrt{z\frac{T}{T_r}}} \qquad \dot{m}' = \frac{\dot{m}\sqrt{\frac{T}{T_r}}}{\frac{p}{p_r}} z^{1.5} \qquad z = \frac{p}{\rho T R_s} \tag{14}$$

Numerical Setup

The standard Peng-Robinson model has been chosen as the cubic state equation for the real gas modeling, given in Eq. 3. This decision is mainly based on comparability considerations concerning the CFD computations which have been carried using a commercial tool during the measurement campaign. Of the available models, the Peng-Robinson EOS showed the smallest error for the chosen working fluid and operating conditions.
In order to account for the temperature dependency of the dynamic viscosity, the interacting sphere model from Chung et al. (1984, 1988) was applied. Furthermore, the thermal conductivity is modeled using the modified Eucken formulation from Reid et al. (1987). The ideal gas contribution of any internal energy change (Path B in Fig. 1) is evaluated using a fourth order polynomial for the specific heat capacity at constant pressure. Turbulence is accounted for by the use of the Menter-SST model (Menter (1994)) with automatic wall treatment. The mesh consists of a total of 9 different regions connected with fourteen interfaces for general grid connections and six in-house developed mixing planes, connecting the regions with different periodicities. Details on the implementation of the used mixing plane can be found in Hanimann et al. (2014). The computational domain consists of 4 mio cells with y^+ values around 20.

Global Performance Comparison

The complete operating range for a given rotational speed was computed using the above described real gas models by continuously increasing the backpressure until the stability limit was reached. In order to access the quality of the results, the solutions are compared against commercial code and measurement results. At the time, the only measurement data available for comparison was the pressure ratio. To validate the implemented procedure, the results are further compared with commercial code results by plotting polytropic efficiency (Eq.15) and work coefficient (Eq. 16) against flow coefficient (Eq. 17). The circumferential velocity u_θ is evaluated at the diameter (D_2) of the first compressor outlet.

$$\eta_p = \frac{\Delta h_{p0}}{h_{0,2} - h_{0,1}} \qquad \Delta h_{p0} = (h_{0,2} - h_{0,1}) - \frac{(s_2 - s_1)(T_{0,2} - T_{0,2})}{ln\left(\frac{T_{0,2}}{T_{0,1}}\right)} \tag{15}$$

$$\lambda = \frac{\Delta h_0}{(u_\theta)^2} \tag{16}$$

$$\Phi = \frac{\dot{V}}{u_\theta (D_2)^2} \tag{17}$$

Figure 3a shows the results for the whole operating range from chocking flow to the stability limit. The legend entries IC and CC stand for the in-house code and commercial code respectively. It is evident that the solutions are in very close agreement, proving the consistency of the underlying thermophysical models. Comparison against measurement data was only available in terms of static pressure ratio, shown in gray. Considering the restrictions of the measurement setup, the values are comparable.

In order to provide a reliable tool for the design of turbomachinery applications operating

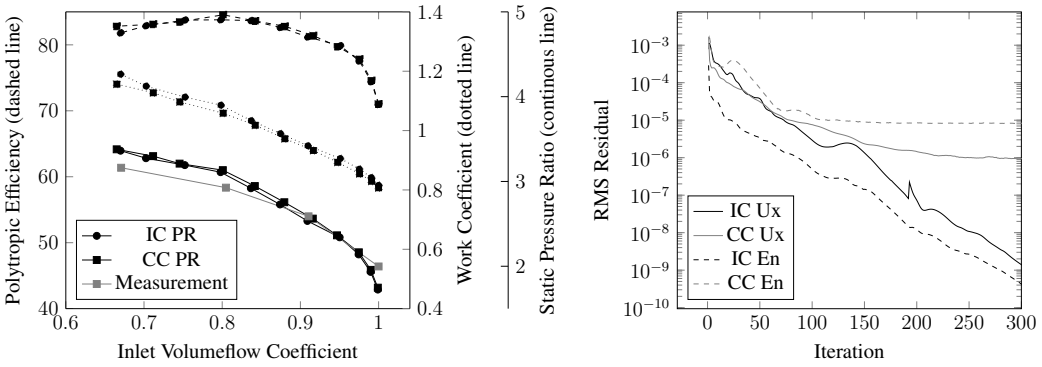

(a) Performance Map Overall System

(b) Convergence History

Figure 3: Two-stage compressor results

in real gas thermophysical regions, accurate numerical solutions solely are not enough. To allow for a high work efficiency and reduced resources it is as important to proof stable convergence behavior with small computational overhead. Investigations considering the convergence behavior have shown promising results as can be seen from Fig 3b. In this figure Ux is the RMS-residual of the momentum equation in x-direction and En the residual of the energy equation. In order to access the effects of real gas modeling compared to perfect gas thermophysical

models, cpu time was compared as well. An increase of about 50% compared when switching to real gas models could be observed for this test case setup. A value well within what is observed from commercial code results.

Real Gas Effects

In this section we only compare solutions obtained with the in-house framework. The investigation focuses on differences in the results when using real gas models instead of perfect gas assumptions. In order to do so, the characteristic was recomputed using standard models for perfect gas as newtonian viscosity, constant heat capacity and Prandtl's law for the conductivity based on average values from the real gas solutions. The results are shown in Fig. 4. Lines with square markers correspond to solutions of the perfect gas model (PG) and lines with circular markers correspond to the real gas solution (RG) based on Peng-Robinson state equation as already shown in Fig. 3a.

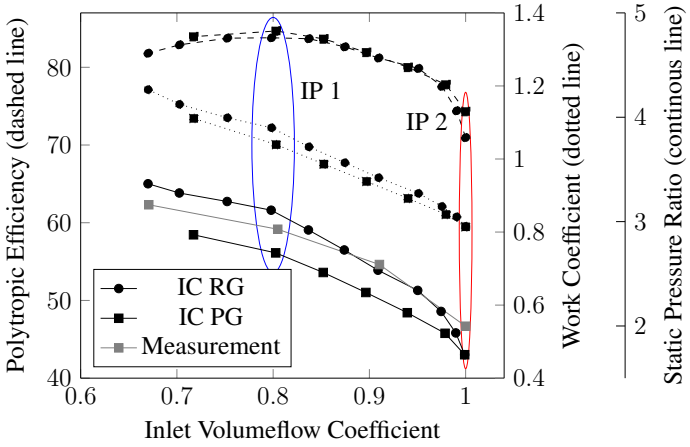

Figure 4: Performance Map: RG vs. PG

Comparing polytropic efficiency, similar results are obtained for flow coefficients above the peak efficiency point. At peak efficiency, a difference of $\sim 2\%$ can be found. While this is surely not negligible, the difference are too small to state any general conclusions.

Comparing the curves of static pressure ratio, it is however clear that for the perfect gas simulations lower back pressure is necessary for the same volume flow coefficient. Using the perfect gas model, it was not possible to reach the same pressure levels as when using the real gas model. Compressor stability limit was detected at much smaller levels of back pressure and the flow coefficient dropped much faster for the perfect gas when increasing the back pressure.

Further investigation of the marked regions (IP1 in blue, IP2 in red) show the differences. IP1 corresponds to peak efficiency for both setups, IP2 are chocking conditions. The operating points of the CFD simulation where set by fixing the value of the pressure at the outlet. As can be seen from IP1 (peak efficiency), to arrive at the same flow coefficient, the perfect gas model needs a much smaller static pressure ratio between inlet and outlet. In fact, the outlet pressure of the perfect gas simulation is roughly 13% lower than for real gas. This is in contrast to IP2 (chocking conditions) where pressure ratio and flow coefficient are in close agreement. Comparing the exit flow angles from Fig. 5a it can be clearly seen that in the first stage, the general orientation between real gas and perfect gas for the same flow coefficient are in close agreement. This is independent whether chocking or peak efficiency is considered. Increasing

deviation can be found when comparing the results in stage 2. An explanation can be found when plotting the average compressibility factor in streamwise direction, see Fig. 5c, showing the increasing deviation from ideal gas state through the compressor. This deviation from perfect gas modeling assumptions become more and more dominant with increasing back pressure, explaining the increased difference in polytropic efficiency for peak efficiency point.

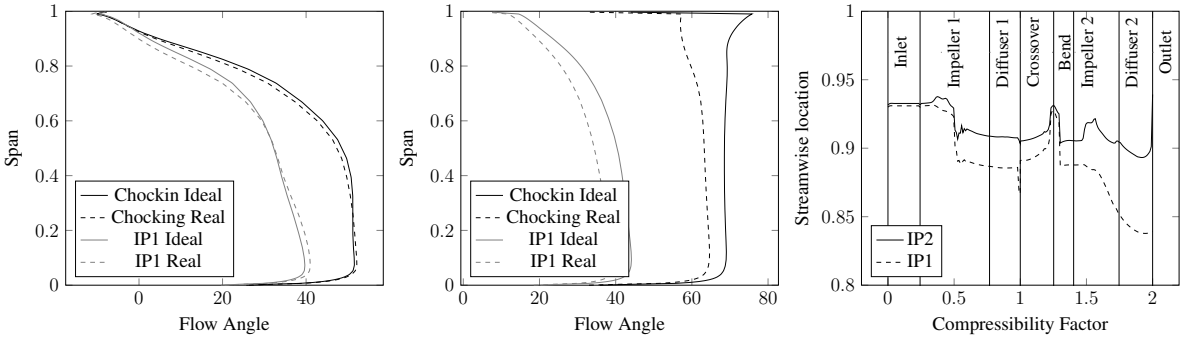

(a) Stage 1 (b) Stage 2 (c) Compressibility

Figure 5: Flow angle and compressibility

A normalized total pressure was computed in order to compare the dynamic contribution between real and perfect gas computations as given in Eq. 18.

$$\bar{p}_0 = \frac{p_0 - \bar{p}}{\bar{p}_0 - \bar{p}} \tag{18}$$

Fig. 6 shows the results for IP1 (Peak efficiency) at sections close to the impeller outlets. For stage 1 results seam comparable, differences however become present in the second stage. This is especially true for the suction side (SS) of the splitter blade (SB), where the dynamic contribution is much lower.

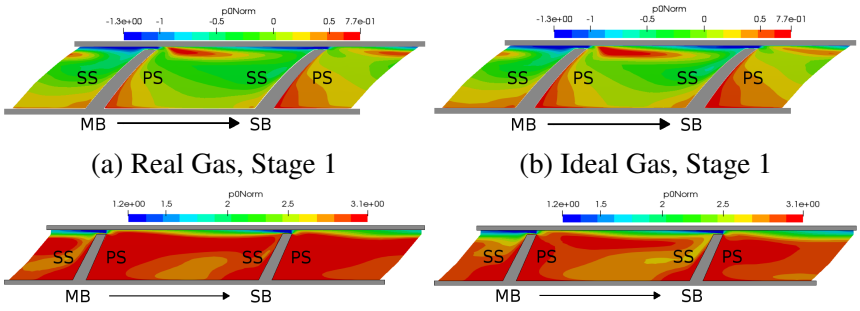

(a) Real Gas, Stage 1 (b) Ideal Gas, Stage 1

(c) Real Gas, Stage 2 (d) Ideal Gas, Stage 2

Figure 6: Normalized Total Pressure Isolines, IP1

The above given insights into the difference of compressor dynamics when switching between real and perfect gas model explain the importance of an accurate representation of the thermophysical properties and derivation of the conservation equations. Using perfect gas models would lead to errors in the design of blade geometries because the flow physics are not captured accurately. It is therefore only an option for preliminary design phase to allow for an increased through put. Detailed analysis would however request for real gas modeling.

CONCLUSIONS

The present work summarizes the necessary steps during the derivation and implementation of Navier-Stokes equations into a pressure based numerical framework when dealing with real gas behavior. The implemented procedure was validated on an industrial type compressor setup and compared against commercial code results and measurement data. It could be proven that the implemented procedure is not only able to accurately replicate commercial code results but also leads to a stability of the iterative scheme that goes beyond the capabilities of the used commercial tool. Comparison against perfect gas assumptions justifies the increased complexity of the implementation. It could be demonstrated based on overall performance prediction and local flow features that the assumption of perfect gas shows its limitation under certain operating conditions, especially away from chocking conditions. Perfect gas assumption can be used to generate initial solutions. Benefit would be an increased CPU time and therefore higher through put. Detailed investigation is however not possible since values as the blade loading would deviate from the actual real gas configuration.

ACKNOWLEDGEMENTS

The authors gratefully acknowledge the financial contribution provided by the Swiss National Science Foundation (SNF). We would also like to express our gratitude to Marwan Darwish from the American University of Beirut (Lebanon) for his encouragement and his valuable help and comments during the process of this work.

References

Ameli, A., Afzalifar, A., Turunen-Saaresti, T. & Backman, J. (2018), 'Effects of real gas model accuracy and operating conditions on supercritical co2 compressor performance and flow field', *Journal of Engineering for Gas Turbines and Power* **140**(6), 062603.

Boncinelli, P., Rubechini, F., Arnone, A., Cecconi, M. & Cortese, C. (2003), Real gas effects in turbomachinery flows: A cfd model for fast computations, *in* 'ASME Turbo Expo 2003, collocated with the 2003 International Joint Power Generation Conference', American Society of Mechanical Engineers, pp. 1103–1112.

Chung, T. H., Ajlan, M., Lee, L. L. & Starling, K. E. (1988), 'Generalized multiparameter correlation for nonpolar and polar fluid transport properties', *Industrial & engineering chemistry research* **27**(4), 671–679.

Chung, T. H., Lee, L. L. & Starling, K. E. (1984), 'Applications of kinetic gas theories and multiparameter correlation for prediction of dilute gas viscosity and thermal conductivity', *Industrial & engineering chemistry fundamentals* **23**(1), 8–13.

Colonna, P., Rebay, S., Harinck, J. & Guardone, A. (2006), Real-gas effects in orc turbine flow simulations: influence of thermodynamic models on flow fields and performance parameters, *in* 'ECCOMAS CFD 2006: Proceedings of the European Conference on Computational Fluid Dynamics, Egmond aan Zee, The Netherlands, September 5-8, 2006', Delft University of Technology; European Community on Computational Methods in Applied Sciences (ECCOMAS).

Hanimann, L., Mangani, L., Casartelli, E., Mokulys, T. & Mauri, S. (2014), 'Development of a

novel mixing plane interface using a fully implicit averaging for stage analysis', *Journal of turbomachinery* **136**(8), 081010.

Lucas, C., Rusche, H., Schroeder, A. & Koehler, J. (2014), 'Numerical investigation of a two-phase co 2 ejector', *International Journal of Refrigeration* **43**, 154–166.

Mangani, L., Buchmayr, M. & Darwish, M. (2014*a*), 'Development of a novel fully coupled solver in openfoam: Steady state incompressible turbulent flows', *Numerical Heat Transfer, Part B: Fundamentals* **66**.

Mangani, L., Buchmayr, M. & Darwish, M. (2014*b*), 'Development of a novel fully coupled solver in openfoam: Steady state incompressible turbulent flows in rotational reference frames', *Numerical Heat Transfer, Part B: Fundamentals* .

Mangani, L., Moukalled, F. & Darwish, M. (2016), 'An openfoam pressure-based coupled cfd solver for turbulent and compressible flows in turbomachinery applications', *Numerical Heat Transfer, Part B: Fundamentals* **NHT15/6608 In printing**.

McBride, B. J., Zehe, M. J. & Gordon, S. (2002), 'Nasa glenn coefficients for calculating thermodynamic properties of individual species'.

Menter, F. R. (1994), 'Two-equation eddy-viscosity turbulence models for engineering applications', *AIAA journal* **32**(8), 1598–1605.

Nederstigt, P. (2017), 'Real gas thermodynamics: and the isentropic behavior of substances'.

Odabaee, M., Sauret, E. & Hooman, K. (2016), 'Cfd simulation of a supercritical carbon dioxide radial-inflow turbine, comparing the results of using real gas equation of estate and real gas property file.', *Applied Mechanics & Materials* **846**.

Peng, D.-Y. & Robinson, D. B. (1976), 'A new two-constant equation of state', *Industrial & Engineering Chemistry Fundamentals* **15**(1), 59–64.

Pohl, S., Jarczyk, M., Pfitzner, M. & Rogg, B. (2013), 'Real gas cfd simulations of hydrogen/oxygen supercritical combustion', *Progress in Propulsion Physics* **4**, 583–614.

Reid, R. C., Prausnitz, J. M. & Poling, B. E. (1987), 'The properties of gases and liquids'.

Rhie, C. & Chow, W. L. (1983), 'Numerical study of the turbulent flow past an airfoil with trailing edge separation', *AIAA journal* **21**(11), 1525–1532.

Soave, G. (1972), 'Equilibrium constants from a modified redlich-kwong equation of state', *Chemical Engineering Science* **27**(6), 1197–1203.

Starzmann, J., Casey, M. M., Mayer, J. F. & Sieverding, F. (2014), 'Wetness loss prediction for a low pressure steam turbine using computational fluid dynamics', *Proceedings of the Institution of Mechanical Engineers, Part A: Journal of Power and Energy* **228**(2), 216–231.

Travis, J., Koch, D. P., Xiao, J. & Xu, Z. (2013), 'Real-gas equations-of-state for the gasflow cfd code', *international journal of hydrogen energy* **38**(19), 8132–8140.